---

**Article:**
Kerrigan, A., Pande, K., Pingstone, D. et al. (5 more authors) (2022) Nano-faceted stabilization of polar-oxide thin films:The case of MgO(111) and NiO(111) surfaces. APPLIED SURFACE SCIENCE. 153490. ISSN 0169-4332

https://doi.org/10.1016/j.apsusc.2022.153490

---

Applied Surface Science 596 (2022) 153490

Contents lists available at ScienceDirect

Applied Surface Science

journal homepage: www.elsevier.com/locate/apsusc

Full length article

# Nano-faceted stabilization of polar-oxide thin films: The case of MgO(111) and NiO(111) surfaces

A. Kerrigan [a], K. Pande [b,c], D. Pingstone [a], S.A. Cavill [a], M. Gajdardziska-Josifovska [b], K.P. McKenna [a], M. Weinert [b], V.K. Lazarov [a,*]

[a] Department of Physics, University of York, Heslington, York, YO10 5DD, State One, United Kingdom
[b] Department of Physics, University of Wisconsin-Milwaukee, Milwaukee, 53211, WI, USA
[c] Molecular Biophysics and Integrated Bio-Imaging Division, Lawrence Berkeley National Laboratory, Berkeley, CA, USA

ARTICLE INFO

*Keywords:*
Thin-film
Polar-oxide
Electron microscopy
First-principles
Nano-faceting

ABSTRACT

Molecular beam epitaxy growth of polar MgO(111) and NiO(111) films demonstrates that surface stabilization of the films is achieved via the formation of neutral nano-faceted surfaces. First-principles modeling of the growth of polar MgO(111) films reveals that the growth does not proceed layer-by-layer. Instead, the Mg or O layers grow up to a critical sub-monolayer coverage, beyond which the growth of the next layer becomes energetically favorable. This non-layer-by-layer growth is accompanied by complex relaxations of atoms both at the surface and in the sub-surface, and leads to the experimentally observed surface nano-faceting of MgO and NiO (111) films through formation of neutral nano-pyramids terminated by {100} facets. These facets are limited in size by an asymptotical surface energy relation to their height; with the reconstruction being much more stable than previously reported surface terminations across a wide range of growth conditions. The termination offers access to lower coordinated atoms at the intersection of the neutral {100} planes whilst also increasing the surface area of the film. The unique electronic structures of these surfaces can be utilized in catalysis, as well for forming unique heterostructures for electronic and spintronic applications.

## 1. Introduction

Polar metal-oxide surfaces are generally unstable, having very high surface energies due to the large electrostatic contribution from the presence of an electric dipole moment in the repeat unit. In a simplified electrostatic picture, the ionic crystal along the polar direction can be viewed as a stack of parallel oppositely charged planes; thus even for thin polar films the electric dipole moment is huge, leading to the so-called 'polar catastrophe'. The electrostatic solution of this problem is offered through various stabilization mechanisms, providing charge modulation of the surface layers via surface atomic and electronic reconstructions [1–3].

Epitaxial oxide growth is an area of technological importance because of the application of ultra-thin oxide films in modern electronics, devices for energy production, catalytic materials, high-temperature superconducting films, and other complex functional materials. Polarity is the main challenge to overcome in the growth of polar oxide films where controllable surfaces and interfaces on the atomic scale are often required. While rock-salt metal-oxide thin films, such as MgO and NiO, are routinely used for a number of applications, including spintronic devices, photovoltaics, and catalysis, a full understanding of the epitaxial growth along the (111) polar direction of these oxides has not been developed, leading to limited application of the polar films. Past studies of MgO(111) thin film growth have demonstrated that atomically flat films, in the presence of H as a surfactant, are achievable [4]. The stabilization of these films, in the bulk unreconstructed MgO(111) surface structure, is due to surface OH termination [5]. However, the epitaxial growth in the absence of surfactants at the microscopic level is not yet fully understood.

In this paper, we present a joint experimental and theoretical study that describes the epitaxial growth of the polar-oxide MgO(111) surface, with emphasis on the physical phenomena that drives film growth while also taking into account the O and Mg chemical potentials. It is well known, from the finite-temperature phase diagram of various oxides and alloys [6–8], that the chemical potential of constituents can vary by several eV as a function of concentration. Most theoretical studies, however, have focused on the stability and stoichiometry of static surfaces in thermodynamic equilibrium [9–11]. Here, we show that during homo-epitaxial growth of the polar MgO(111) surface there is a variation of the Mg and O chemical potentials as a function of

* Corresponding author.
*E-mail address:* vlado.lazarov@york.ac.uk (V.K. Lazarov).

https://doi.org/10.1016/j.apsusc.2022.153490
Received 26 January 2022; Received in revised form 20 April 2022; Accepted 23 April 2022
Available online 30 April 2022

concentration, which is the driving force for continued growth. Since the chemical potentials are a measure of each component's contribution to the energy of formation, the O(Mg) layer is relatively more binding in Mg(O)-rich regions, and preferential growth of Mg or O on a surface at a given stoichiometry is determined by their relative binding energy. In the case of MgO(111) an O(Mg) layer begins growing on top of the partially formed Mg(O) layer following a multi-layer growth pattern as opposed to the expected strict layer-by-layer epitaxial (Frank–Van der Merwe) growth mode. Despite the growth being multi-layered, there is no intermixing of Mg and O atoms within each layer. The surface and subsurface Mg and O atoms in MgO(111) films show large relaxations, that are meta-stable in nature, as more layers are deposited, the displaced atoms relax back into their respective ideal positions. As a result, the roughness and defects, in the form of vacancies and adatoms, are confined to a few layers on the surface, and the "bulk" of the film is defect free and preserves the rock-salt FCC stacking sequence. These calculations are consistent with the experimentally observed 3D growth of the MgO(111) films during Molecular Beam Epitaxy (MBE) growth, including the lack of full wetting layers. In addition, we show that other MBE grown rock-salt oxides films, such as NiO(111), show the same surface structure, consisting of nano-faceted pyramids truncated by {100} type of surfaces, as the main surface stabilization mechanism.

## 2. Experimental methods

The MgO(111) and NiO(111) films were grown by MBE on 6*H*-SiC(0001) and MgO(111) substrates, respectively. Preparation of the SiC substrates was performed in the MBE chamber by heating to 900 °C under a flow of molecular hydrogen for 30 min. The MgO(111) substrates were prepared *ex-situ* by heating to 1000 °C in an open atmosphere for 1 h in a furnace before being transferred to the MBE chamber. These substrates were chosen for the low lattice mismatch they provide with the MgO(111) and NiO(111) films grown, 3% and 1% respectively.

*In-situ* characterization of the substrates by reflection high-energy electron diffraction (RHEED) and low-energy electron diffraction (LEED) showed a surface reconstruction and improved flatness after hydrogen cleaning. The films were co-deposited by simultaneous exposure of the substrate to oxygen and either magnesium or nickel vapors. Createc effusion cells set to 280 °C and 1300 °C were used as sources of Mg and Ni atoms, respectively. Oxygen was provided from the Oxford Applied HD-25 Oxygen Plasma source operating at low power (less than 100 W). The oxygen pressure in the chamber was $10^{-6}$ mbar. The SiC substrate was heated by DC resistive heating and held at 500 °C, while the MgO substrate was held at 300 °C. After deposition of the films, the samples were analyzed *in-situ* with RHEED and LEED. Cross-sectional structural analysis of the films was performed by transmission electron microscopy (TEM). The TEM specimen preparation was done by conventional methods including mechanical thinning and polishing followed by the precision ion milling process. TEM images were acquired on a 200 kV JEOL 2011 TEM, and double aberration corrected 2200FS JEOL TEM.

## 3. Computational methods

We model the homoepitaxial growth process of ultrathin MgO films on self-standing unreconstructed polar MgO(111) slabs. This is important even though the experimental growth is heteroepitaxial, since factors such as lattice mismatch and substrate roughness would be excluded for promoting non-laminar growth. Calculations were performed using the full-potential linearized augmented plane waves method (FLAPW) as implemented in FLAIR with the generalized gradient approximation (GGA) functional of Perdew–Burke–Ernzerhof (PBE) [12–15]. Calculations for the surface are modeled by repeated layers of Mg and O. The two surfaces of the slabs are identical to maintain inversion symmetry and sufficient vacuum (greater than 15 Å) is left between the two surfaces so that the surface-surface interactions through both the vacuum and slab are negligible. The model growth calculations use a 3 × 3 supercell of the (111) primitive cell with 9 layers for Mg-terminated and 11 layers for O-terminated MgO(111) surfaces. For all cases, the calculated lattice constant $a_{cubic}$ = 4.19 Å ($a_{hex}$ = 5.13 Å) was used, and allowed full structural relaxations until the forces were smaller than 0.0005 htr/a.u. (~0.025 eV / Å). The Brillouin zone integration was performed with a 5 × 5 ×1 k-point grid. Since epitaxial growth is a non-equilibrium technique that involves a flux of species onto and from the surface, the method of *ab-initio* thermodynamics, suitable for investigation of equilibrium surface reconstructions, is not suitable for modeling growth. Therefore, we adopted a different approach, as follows. The chemical potential of the constituent species in a system (bulk/surface/interface) is defined as the energy required to add a single atom of a constituent species to the system, i.e.

$$\begin{aligned}\mu_i &= \left(\frac{\partial G}{\partial n_i}\right)_{T,p} \\ &= \frac{G\left(N_i+\Delta n_i, N_j\right) - G\left(N_i, N_j\right) - \Delta n_i G_i^0}{\Delta n_i} \\ &= E_i^{\text{ads}} \end{aligned} \quad (1)$$

where $G(N_i, N_j)$ is the Gibbs free energy of a system with $N_i$ and $N_j$ atoms of constituents $i$ and $j$, respectively, $E_i^{\text{ads}}$ is the adsorption energy of $i$ and $G_i^0$ is its energy per atom in the bulk (reference) phase. The Gibbs free energies are approximated by the total energies from DFT calculations, ignoring vibrational entropy contributions for simplicity. Here, $\mu_O$ and $\mu_{Mg}$ are referenced to half the energy of molecular oxygen and the energy of metallic Mg, respectively, which directly equates chemical potential to adsorption energy. Therefore, in the thermodynamic limit, the chemical potential of species $i$ is given as the finite difference approximation of the Gibbs free energy per atom of systems with $N_i$ and $N_i+\Delta n_i$ number of atoms of $i$, keeping the number of atoms of all other species constant. Eq. (1) explicitly shows that the chemical potentials of the components in a system are dependent on its instantaneous stoichiometry, even though the external conditions remain constant. We approach the problem of describing layer-by-layer growth by calculating the adsorption energy $E^{\text{ads}}$ for a single Mg or O atom at different surface coverage. If the adsorption energy (chemical potential) is negative then the growth of that particular species is favorable, otherwise it is not.

The faceted surface reconstruction of MgO and NiO is modeled using VASP and PAW-PBE potentials [16–19]. The structures were prepared with a 4 × 4 reconstructions on either side of the surface slab. The cell consisted of 23 layers in total, with the reconstruction requiring 9 layers. For NiO an effective Hubbard U parameter of 5.3 eV was used as this parameter and functional were shown to describe the ground state of bulk NiO as well as (100) surfaces well [20]. The surface energy calculations were performed relative to bulk NiO and MgO cells consisting of the same number of atoms and identical a-vector and b-vector to the reconstructed supercell, as well as an isolated $H_2O$ molecule in the case of the OH-terminated surface. As in the previous calculations, a 15 Å vacuum gap was used to reduce the interaction between the repeated images.

## 4. Experimental results

Fig. 1a shows the RHEED pattern of the SiC(0001) surface along the [11$\bar{2}$] direction. The streaky RHEED pattern indicates atomically flat substrate surface. In contrast, the RHEED from the grown MgO(111) film surface (Fig. 1b) consists of transmission spots aligned along with the expected positions of the [11$\bar{2}$] film streaks, which indicates a 3D island growth of the MgO film, i.e., formation of a rough/faceted film surface. Morphology and orientation of the MgO(111) film facets is determined by undertaking LEED and TEM studies of the MgO films.

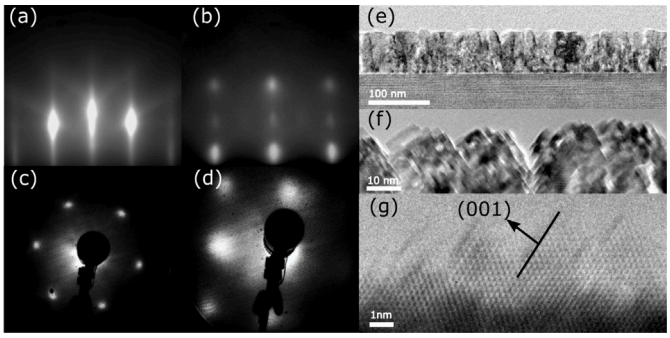


**Fig. 1.** RHEED, LEED and TEM images of MgO (111) thin films on SiC (0001). (a) RHEED pattern of the SiC(0001) surface along the [11-2] direction. (b) RHEED from the grown MgO (111) film. (c) LEED from the film acquired with beam perpendicular and (d) sample tilted to 54.7°. (e) Bright-field TEM image with larger field of view displaying a sharp interface between the MgO film and the SiC substrate, and (f) the faceting of the film surface with nanometer-scale features. (g) HRTEM image of the faceted surface, the angle between faceted planes and the (111) planes is outlined, showing the {100} terminated facets in (d).

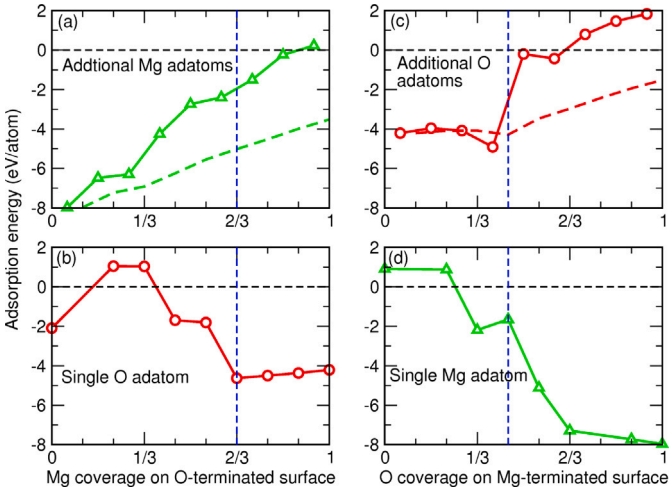


**Fig. 2.** The adsorption energies of (a) additional Mg adatoms, and (b) single O adatom as a function of Mg coverage on an O-terminated (1 × 1)-MgO(111) surface; of (c) additional O adatoms, and (d) single Mg adatom as a function of O coverage on an Mg-terminated terminated (1 × 1)-MgO(111) surface. Vertical dashed lines in (a) and (b) show the Mg coverage at which an O adatom becomes more binding (on the incomplete Mg layer) than a Mg adatom. Similarly, vertical dashed lines in (c) and (d) show the O coverage at which Mg adsorption (on the incomplete O layer) is more favorable than O adsorption. The green and red dashed lines in (a) and (c) are the average per atom of all the additional adsorption energies. Coverage here is relative to the (3 × 3) supercell and as such full coverage is 9 atoms.

The LEED pattern recorded with the incident electron beam directed along the normal of the surface is shown in Fig. 1c. A six-fold diffraction pattern, as expected from a MgO(111)—(1 × 1) surface, is clearly observed. However, when the energy of the electron beam is increased, the diffraction spots move outwards, indicating that observed hexagonal pattern might also originate from trigonal faceted surface islands. Indeed, when the specimen was tilted by 54.7°, we observe a LEED diffraction pattern with square symmetry. The specific angle of rotation brings (100) type surface facets in a position normal to the incident electron beam, hence the observed square symmetry of the LEED pattern in Fig. 1d.

A direct confirmation, in real space, of the LEED results, and overall film morphology is further provided by cross-sectional TEM of the grown MgO(111) film. The bright-field image at low magnification reveals a sharp interface between the MgO film and SiC, Fig. 1e. The single crystal structure of the grown film and the epitaxial crystallographic relation of the film and substrate is given by MgO(111)‖SiC(0001) and MgO(11$\bar{2}$)‖SiC(11$\bar{2}$0). A close view of the surface (Fig. 1f) shows the faceted nature of the MgO(111) surface. The HRTEM image of the MgO surface (Fig. 1g) provides visualization of the atomic planes of the film surface along [1$\bar{1}$0] direction. The angle between the faceted surface planes and the (111) planes (54.7°), corresponds to the expected angle between (111) and (100) planes. These results directly confirm the RHEED/LEED results, and clearly show that the polar MgO(111) film growth mode is 3D, and that the surface faceting into nano-pyramids is determined by neutral {100} type of planes. Next we present the modeling associated with the MgO(111) growth in order to elucidate the driving force behind the observed surface faceting, and further show that nano-faceting into neutral surfaces is inherent to the polar film growth process.

## 5. Growth modeling

Numerous previous studies have applied atomistic thermodynamics approaches based on density functional theory (DFT) to describe systems in thermodynamic equilibrium, taking into account the effect of the atmosphere or "environment" (e.g. a gas phase of one or more species) through the chemical potential [21–28]. In thermal equilibrium, the chemical potential, which is the driving force for growth, can be related to the partial pressure and temperature of the growth, and as such the chemical potential can be controlled externally, for example, by choosing the appropriate temperature and oxygen partial pressure. Hence the relative stability of *static* surfaces with different stoichiometries and in thermodynamic equilibrium with separate reference phases can be estimated by searching for the configuration with the lowest Gibbs free energy. Epitaxial growth, on the other hand, is a highly non-equilibrium technique that involves a flux of constituents onto and from the surface that is undergoing a continuous change in stoichiometry. MgO(111) consists of alternating layers of Mg and O in the fcc ABC-type stacking along the [111] direction. As a result, bulk-terminated MgO(111) is not charge neutral, and has a non-zero dipole moment along the surface normal. The first question we address is which of the various available sites for adsorption of Mg(O) atoms on O(Mg)-terminated surfaces are energetically favorable, i.e., what stacking sequence is preferred. For the case of Mg adsorption on an O-terminated surface with O occupying the A sites and the subsurface Mg atoms in B sites, the C site is preferred over the B site by 0.23 eV/atom at the start of Mg-layer growth, and by 8.2 eV/atom and 2.3 eV/atom at a one-third and two-third Mg coverage, respectively, thus maintaining the ABC stacking sequence of the fcc structure. Similarly, for O adsorption on a Mg-terminated surface with Mg atoms in C sites, the ideal B site in conformity with the fcc stacking is preferred over the stacking fault site by 0.5 eV/atom at no O coverage and 7.1 eV/atom at one-third coverage. Thus the bulk MgO fcc stacking is preserved throughout the growth. Island nucleation is often the first step in the formation of an adlayer, and as the surface coverage increases it is more likely for the adatoms to deposit next to the stable islands and promote their growth instead of forming new nuclei. Our calculations show that at a one-third Mg coverage, the adsorption of Mg atoms in nearest neighbor sites (forming a triangular cluster) is preferred over adsorption at other sites by 0.4 eV/atom. Such tendency for clustering is even stronger in the case of O, where the formation of a triangular cluster is more favorable by 2.2 eV/atom. As more adatoms are added, they prefer to deposit close to the already formed clusters rather than at an isolated site. These results would suggest a preference for a layer by layer growth in the polar direction, but further modeling reveals complexities, as shown in the following detailed modeling.

Next, we consider the growth process of MgO(111) films. We start with epitaxial growth in a controlled environment considering first the simpler case when there is an influx of either one of the two components, simulated as adsorption of only Mg(O) on a stoichiometric O(Mg) terminated surface. The more complicated case of growth in the

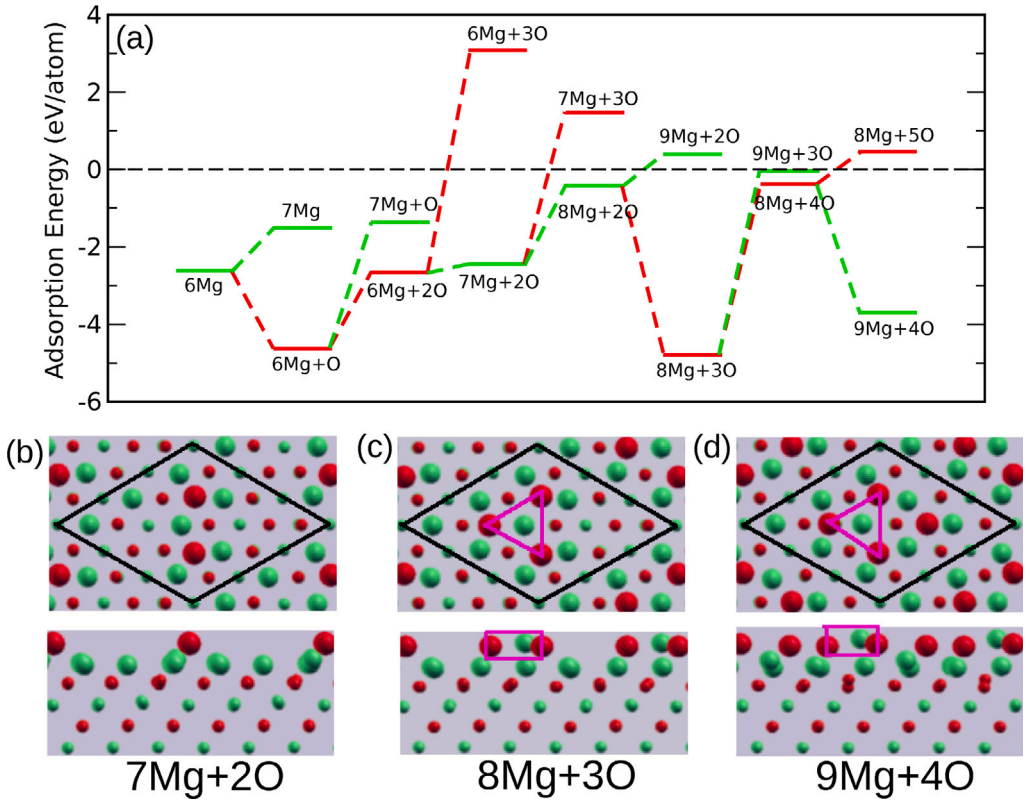


**Fig. 3.** The adsorption energy of Mg and O adatoms for different structures that form during the growth of a complete Mg layer on O-terminated (1 × 1) MgO(111). Top and side views of structures with (b) 7 Mg atoms in the Mg and 2 O atoms in the next O layer, (c) 8 Mg atoms in the Mg and 3 O atoms in the next O layer, and (d) 9 Mg atoms in the Mg and 4 O atoms in the next O layer. Calculations are done for a (3 × 3) supercell as shown by the black outline. Green (light) and red (dark) spheres represent Mg and O atoms, respectively. Mg atom at the center of the magenta triangle in (c) and (d) moves out of the Mg plane through the O layer upon structural relaxations (cf. Fig. 5).

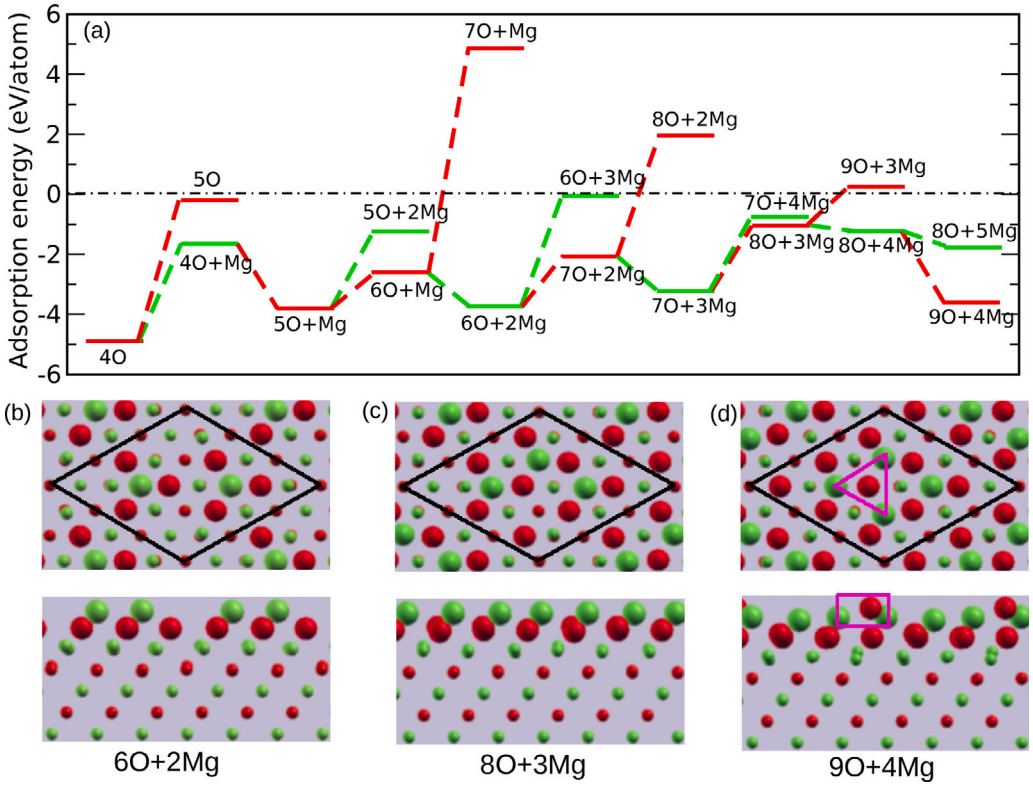


**Fig. 4.** The adsorption energy of Mg and O adatoms for different structures that form during the growth of a complete O layer on Mg-terminated (1 × 1) MgO(111). Top and side views of structures with (b) 6 O atoms in the O and 2 Mg atoms in the next Mg layer, (c) 8 O atoms in the O and 3 Mg atoms in the next Mg layer, and (d) O-terminated MgO(111) with 4 Mg atoms. Calculations are done for a (3 × 3) supercell as shown by the black outline. Green (light) and red (dark) spheres represent Mg and O atoms, respectively.

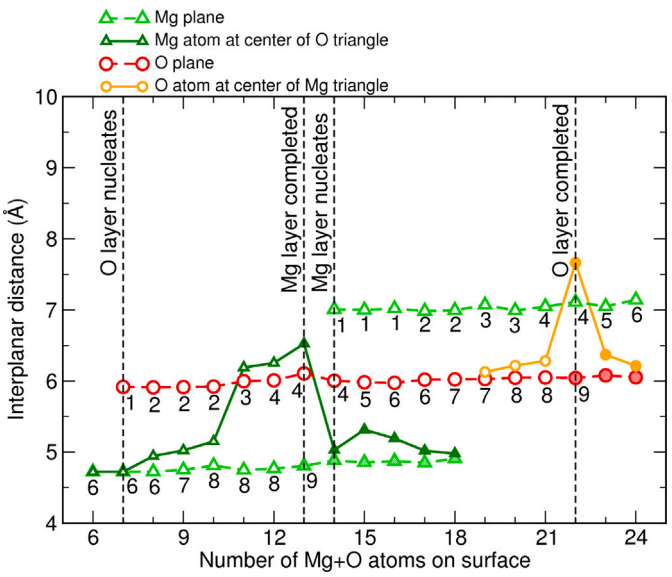


**Fig. 5.** Displacement in Å along the surface normal of the Mg plane (light green triangles), Mg atom (dark green triangles) at the center of a triangular O cluster (red circles), O plane (red circles) and O atom (orange circles) at the center of an Mg triangular cluster (green triangles). The calculated Mg-O interplanar distance along the surface normal is 1.21 Å. Filled triangles (circles) represent Mg (O) atoms in completed (with 9 atoms) Mg (O) layer. Note that the next O (Mg) layer starts nucleating before the previous Mg (O) layer is completely formed, but there is no intermixing between Mg and O atoms within a layer.

simultaneous flux of both Mg and O is considered later. Figs. 2a and 2c show adsorption energies for successive Mg and O atoms for the lowest energy adsorption sites at $T = 0$ as a function of the number of Mg and O atoms deposited at the surface. Starting on a stoichiometric O-terminated surface, Mg adsorption remains favorable until the surface has 8 out of 9 sites occupied, at which point the energy cost for adding the last Mg adatom to complete the monolayer is 0.24 eV/atom. On the other hand, starting on a completely Mg-terminated surface with only atomic oxygen in the environment, we find that the adsorption energy for O remains negative (i.e., O adsorption is favorable) until two-thirds O coverage on the surface. The adsorption energies (chemical potentials) tend to become less binding as the layers approach completion, and once they become positive the growth of full layers will stop, thereby leaving vacancies and defects in the film. However, the films in this study, as well as other layer-by-layer grown MgO(111) films on various substrates, appear to consist of well-defined alternating layers of Mg and O that are largely defect-free except at the surface where there are indications of the presence of islands, terraces, and step structures. Therefore, there should be some mechanism through which the vacancies in Mg and O layers get filled to yield defect-free films. Figs. 2b and 2d show adsorption energies for single O and Mg adatoms, respectively, as a function of Mg and O concentration on the surface. If both Mg and O sources are available in the growth chamber, then at two-third Mg coverage the next O layer starts forming in preference to further Mg growth, and analogously at almost one-half O coverage, the formation of the next Mg layer becomes more favorable than completion of the O layer. Motivated by these results, we now consider a (multi) layer-by-layer growth mechanism (under the simultaneous flux of Mg and O atoms) in which the next O(Mg) layer starts forming on top of the partially formed Mg(O) layer, and show that such a growth mode indeed promotes completion of the layers, giving rise to defect-free alternating metal and oxygen planes. Since the number of possible surface configurations for such an approach is very large, we will restrict our analysis to the most favorable (lowest energy) process.

Consider that the growth starts on a stoichiometric O-terminated surface of MgO(111). At the start of the growth of the Mg monolayer, the adsorption energy of both Mg and O adatoms at the same time is −3.8 eV/atom if O occupies one of the vacant Mg sites and −2.7 eV/atom if O goes in its ideal site in the layer above Mg, both of which are much less than the adsorption energy of only Mg adatoms as shown in Fig. 2. This is reasonable since each monolayer in the [111] direction consists of only Mg or O atoms, thus if O adsorbs in the same layer as Mg, which is on the top of an O monolayer, the O adatom is bonded to other O atoms, whereas if O adsorbs in the layer above Mg it does not have enough Mg atoms (at low Mg coverage) to bond with. As shown before (see Fig. 2), the adsorption of Mg adatoms proceeds until two-third Mg coverage, at which point positioning of an O adatom in an ideal fcc site in the layer above the incomplete Mg layer becomes energetically more favorable ($\Delta E_O = -4.63$ eV) than further growth of the Mg layer, which initiates the formation of the next O adlayer. The preferred site for O nucleation is in a hollow site above the Mg island rather than a vacant site in the incomplete layer. As shown in Fig. 3, after O nucleation the following two processes are possible: (*i*) Mg adsorption in the incomplete Mg layer with $\Delta E = -1.36$ eV/atom, leading to 7Mg + O structure, and (*ii*) continuation of the growth of O adlayer (6Mg + 2O structure) by deposition of another O adatom. For the latter process the adsorption energy for the O atom is −2.66 eV/atom when it is in a nearest neighbor site to the first adatom and −1.69 eV/atom when it is farther away (not shown in the figure), showing a preference toward clustering rather than random nucleation. At this point, an Mg atom which is bonded to both O atoms in the adlayer starts moving out of its ideal plane toward the surface. The quasi-equilibrium nature of the growth process manifests in the relaxations of the newly adsorbed atoms on the surface — the adsorption energy does not totally represent the binding energy of the atom to the structure, but a part of it comes from the motion of the adatoms. The next two energetically favorable steps are the adsorption of Mg atoms in two out of the remaining three vacant sites with a binding energy of 2.44 and 0.41 eV/atom, respectively, which leaves just one vacant site in the Mg layer (8Mg + 2O). While the cost of completing the Mg layer by filling the last site is 0.4 eV/atom, it is favorable to add two more O adatoms to the O cluster above the Mg layer. In the presence of this four atom O cluster, the adsorption energy for the last Mg atom is −3.4 eV/atom, resulting in a stoichiometric Mg-terminated MgO(111) surface with a partially formed O layer (9Mg + 4O).

Next we consider the growth of the O layer on a stoichiometric Mg-terminated MgO(111) surface. We see from Figs. 2 and 4 that at almost one-half O coverage a Mg adatom adsorbs in an ideal fcc site on top of the O layer in preference to another O atom being added to the existing O cluster ($\Delta E_{\mathrm{Mg}} = -1.65$ eV/atom vs $\Delta E_{\mathrm{O}} = -0.2$ eV/atom). Even though there are enough vacant sites in the O layer, an Mg atom initially sitting in one of these vacant sites has a tendency to move out of the plane upon relaxations due to interactions with the Mg atoms in what is now the sub-surface Mg layer, ruling out intermixing of Mg and O within a plane. The next steps in the growth process are the preferential adsorption of two more O atoms near the four atom cluster with $\Delta E = -3.8$ eV/atom vs $\Delta E = -2.6$ eV/atom, respectively, followed by a second Mg adatom nearest neighbor to the one already nucleated with a binding energy of 3.7 eV/atom. The surface has two triangular clusters of oxygen, thus giving a two-third O coverage, with an Mg adatom at the center and on top of each of the two clusters (6O + 2Mg). The remaining three vacancies in the O layer are filled by alternate adsorption of O and Mg in their respective ideal sites (and layers) and the resulting structure looks like an ideal O-terminated MgO(111) surface with the next Mg adlayer on top (9O + 4Mg).

While at first glance, the thermodynamic pathways for the formation of complete Mg and O layers as outlined in Figs. 3 and 4, respectively, might appear to be disconnected or independent of each other, in Fig. 5 we show how a scenario with the two pathways

can come together to describe a continuous chain of events, i.e., film growth. The *x*-axis shows the total number of Mg and O atoms added to the surface, and *y*-axis shows the position of the atoms in the [111] growth direction. Open (filled) triangles and circles show Mg and O atoms, respectively, in a layer with fractional (complete) coverage. By virtue of the metastable nature of the growth process, the atoms at the surface and sub-surface are not static and undergo significant relaxations as a response to the continuous change in surface stoichiometry and structure. The motion of Mg and O atoms does not freeze once the layers are "completed", as shown by the large relaxations of the filled triangles and circles.

During the growth of the Mg layer, an O adlayer starts nucleating at two-thirds Mg coverage and triggers outward motion of the Mg atom nearest neighbor to the O adatoms. As already discussed above, the growth takes place by adsorption of atoms to the already existing cluster/island in preference to adsorption at isolated sites. When the surface has 8 Mg atoms with a triangular O cluster on top ($N_{ads}$ = 11), the Mg atom at the center of the O trimer (Fig. 3c) moves completely through the O plane by a distance greater than the ideal interplanar distance of 1.21 Å and continues this upward movement when another O and Mg adatom is added to the film. Even though at this point ($N_{ads}$ = 13) 9 Mg atoms have been added to the film (which is the exact number of atoms required to complete the Mg layer), the displacement of an Mg atom through the O plane to the surface of the film creates a vacancy in the Mg layer. As seen in the figure, the next step in the growth process ($N_{ads}$ = 14) is the preferential adsorption of a new Mg atom on top of the partially formed O layer, and this triggers the Mg atom displaced from the sub-surface to move downward back into its ideal plane. As the O and Mg layers continue to grow, at $N_{ads}$ = 22 an O atom sitting at the center of the Mg trimer (Fig. 4d) moves outward through the Mg plane to the surface of the film, hence creating a vacancy in the O layer. This displaced O moves back into its ideal plane as the Mg coverage increases. It is evident from the magnitude of atomic displacements that the top three layers at the surface are neither atomically flat nor free of vacancies. However, with progressive growth in the [111] direction, the layers in the "bulk" of the film become approximately static and defect-free. A critical observation here is that once 9 Mg and 9 O atoms (i.e. a complete MgO unit for a 3 × 3 supercell) have been added to the surface, the surface structure that we end with at $N_{ads}$ = 24, is identical to the one that we started at $N_{ads}$ = 6, thereby ensuring that continuity of the growth is maintained. The extent of atomic relaxations at the (111) surface could be a response of the film to the dipole field (see Supplementary Material) that exists in the [111] direction since similar simulations performed for the non-polar MgO(001) surface (see Supplementary Material) reveal much smaller relaxations of adatoms during the growth process.

## 6. Discussion

During growth, it is highly probable that there are multiple degenerate non-equilibrium pathways through which growth takes place; as such, the process outlined above is not the sole method in which the layer-by-layer growth of MgO(111) films can continue. Several experimental studies have shown initial laminar like growth of MgO(111) films [29,30] that is suppressed by a 3D growth with an increase of the film thickness [30]; although flat films can be grown when a surfactant is present [4]. The existence of degenerate structures is especially likely when the Mg and O layers are almost completely filled. For example, during the growth of the O layer when the surface has eight O atoms and a four Mg atom adlayer, the adsorption energy for an O atom in the layer above Mg island is 3.7 eV/atom while that for O in the incomplete O layer is 3.6 eV/atom. If the growth follows the former step, the last vacancy in the O layer is still filled with a binding energy of 1.0 eV, and the final structure would look like it has a half-monolayer Mg coverage with an O nucleus on a stoichiometric O-terminated surface. This shows that the multi-layer-by-layer growth process is highly complex and involves changes in both the stoichiometry and structure of several layers near the surface during the growth. An important implication of the presented theoretical study is that the surface of the film may not have a uniform structure and that regions with different local atomic configurations may be present at the surface. However, the non-uniformity and roughness are limited only to the surface layers, while the "bulk" of the film consists of defect-free and atomically flat alternating planes of Mg and O. The calculations indicate that the surface of MgO(111) film can have a variety of structures strongly dependent on the chemical environment, and since the Mg and O layers grow simultaneously and show significant relaxations, reconstruction of the surface is not limited to the topmost layer but can extend to several layers at the surface. These results correlate well with the growth data presented previously indicating the formation of incomplete surface layers, i.e., nanosized surface islands that are terminated with neutral {100} surfaces which reduce the overall surface energy of the film.

The tendency to form new atomic layers before the completion of the previous layer is a direct consequence of the surface dipole moment contribution to the surface energy, thus is expected to be present in other rock-salt polar-oxide films. Indeed, the experimental results on the surface structure of MBE grown NiO(111) films confirm this expectation. Fig. 6 shows a cross-section TEM image of a polar NiO(111) film. The surface of the film shows the characteristic nano-pyramidal islands

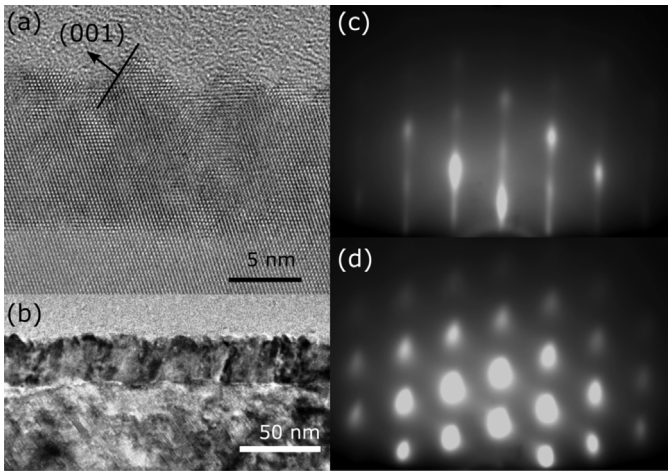


**Fig. 6.** TEM and RHEED images of a NiO(111) film grown on MgO(111). (a) Nanometer scale features on the surface are {100} facets, shown by the angle facet with the (111) surface, creating pyramid like structures. (b) Lower magnification TEM image of the same film showing extended vertical grains. (c) Shows the RHEED pattern of the MgO(111) substrate before deposition, displaying clear streaks indicating a flat surface. (d) Shows the RHEED pattern for the NiO(111) film with electron diffraction spots visible. These spots indicate that the surface is textured 3D growth, as shown in (a) and (b).

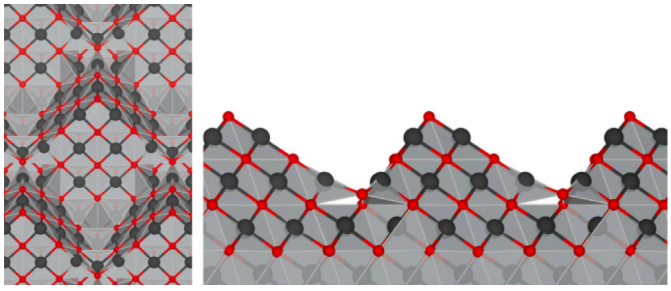

**Fig. 7.** Images of a fully relaxed, oxygen terminated, {100} faceted (111) surface simulation cell. Cations are displayed in black, anions in red. The left panel shows a top down view, slightly off axis to accentuate the facets of the surface. In the right panel, the cell is viewed down the [1$\bar{1}$0] axis and shows the raising of the saddle points where the pyramids meet.

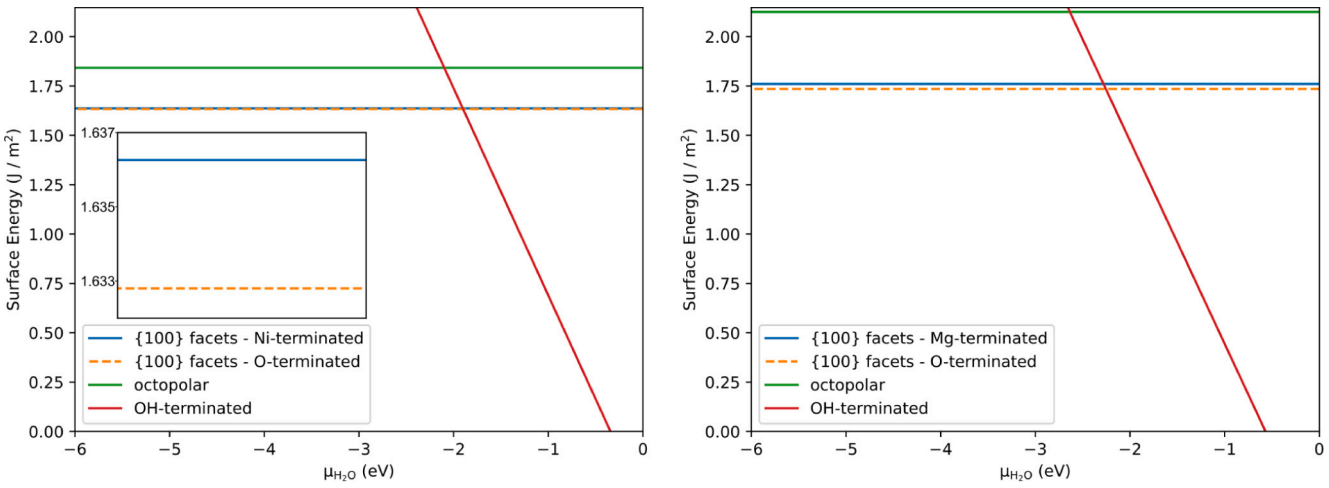


**Fig. 8.** Surface energy of various reconstructions of the (111) surface of NiO (left) and MgO (right), with respect to the $H_2O$ chemical potential. The inset for NiO (common horizontal axis) highlights the difference between O and Ni terminations of the faceted surface.

terminated with {100} facets, similar to the surface of the MgO (111) film shown in Fig. 1. The RHEED of the MgO(111) substrate and surface of the NiO(111) film show diffraction rods and transmission spots from the substrate and film, respectively, indicating flat substrate surface and faceted film surface. These results show that the driving force behind the growth of both films is generic and is inherently connected to the polarity of both NiO(111) and MgO(111) surfaces. This conclusion is further strengthened by calculations modeling the growth of MgO along the neutral [001] direction (see Supplementary Material), where it is shown that layer-by-layer growth is energetically favorable. The experimentally observed {100} faceted pyramids on both MgO and NiO are consistent with the fact that {100} extended surfaces are neutral and have the lowest surface energy.

In the literature there are a number of reconstructions reported for both NiO(111) and MgO(111) [31,32]. Among them the octopolar and OH reconstructions have the lowest surface energies, as such, it is useful to consider how the nano-faceted reconstruction described in this work compare to these reconstructions. Fig. 7 shows the relaxed coordinates of the model used to simulate the {100} faceted (111) surface of both MgO and NiO. The surface energy of these structures are compared to the surface energy of the octopolar reconstruction and hydroxylated surface for MgO and NiO with respect to $H_2O$ chemical potential, which allows us to include comparison with OH terminated surfaces.

Fig. 8 shows the surface energy of chosen reconstructions with respect to $H_2O$ chemical potential. It is clear that neutral-faceted reconstruction is more favorable for both NiO and MgO across a wide range of $H_2O$ chemical potential, supporting previous work indicating high water-vapor pressure was required to hydroxylate the surface of MgO(111) [33]. We note that the size of the surface pyramids does not change the ratio between the total surface areas of (100) facets and their bases (i.e., pyramids footprint). Therefore, the increase of pyramids height asymptotically approaches a scalar multiple of the neutral (100) surface energy. This simple geometrical argument can explain why one finds facets with nano-pyramids of well defined size since there is little energetic gain with an increase of the facet size.

## 7. Conclusions

In contrast to the growth of oxides along non-polar directions, i.e., [001] for rock-salt MgO and NiO, where the structure and atomically sharp surfaces are well controlled, the growth of NiO and MgO along the polar [111] direction is more complex due to the presence of a large surface dipole moment in repeat unit cell. When considering layer-by-layer growth of MgO(111), the DFT modeling shows that completion of either O and Mg layer is not favored. Instead, a growth that promotes an island formation is preferred in which starting a new layer occurs before the completion of the previous layer. Further, we have shown that the growth pathway for continuous polar MgO films is energetically feasible with several layers of the surface reconstructed. Experimentally the growth dynamics of the polar films is driven by both thermodynamic and kinetic constraints. The MBE growth of both MgO(111) and NiO(111) films show that the growth is quasi 2D multi-layer-by-layer resulting in a 3D film termination such that both films are stabilized via formation of nano-sized trigonal pyramids terminated with neutral {100} facets. The experimentally observed growth mechanism can be understood as a combination of the two growth scenarios considered theoretically, the simultaneous absorption of metal and oxygen and the subsequent growth of metal and oxygen layers. We further show that the nanofaceted reconstruction is favorable compared to the low energy octopolar and OH surface reconstructions, for a large range of $H_2O$ chemical potentials, for both MgO and NiO. Finally, we note that polar MgO and NiO films with controlled nanofaceted geometry can provide a good platform for catalysis due to low coordination of atoms in the exposed {100} facets.

## CRediT authorship contribution statement

**A. Kerrigan:** Investigation, Visualization, Writing – original draft, Formal analysis. **K. Pande:** Visualization, Investigation, Formal analysis. **D. Pingstone:** Investigation. **S.A. Cavill:** Writing – review & editing. **M. Gajdardziska-Josifovska:** Writing – review & editing, Supervision. **K.P. McKenna:** Writing – review & editing, Project administration, Supervision, Resources. **M. Weinert:** Writing – review & editing, Visualization, Supervision. **V.K. Lazarov:** Writing – review & editing, Project administration, Conceptualization, Supervision, Resources.

## Declaration of competing interest

The authors declare that they have no known competing financial interests or personal relationships that could have appeared to influence the work reported in this paper.

## Acknowledgments

This work was supported by the Engineering and Physical Sciences Research Council (EP/N509802/1). Some of this project was undertaken on the Viking Cluster, which is a high performance compute facility provided by the University of York. We are grateful for computational support from the University of York High Performance Computing service, Viking and the Research Computing team.

## Appendix A. Supplementary data

Supplementary material related to this article can be found online at https://doi.org/10.1016/j.apsusc.2022.153490.

## References


[1] C. Noguera, Polar oxide surfaces, J. Phys.: Condens. Matter 12 (31) (2000) R367–R410, http://dx.doi.org/10.1088/0953-8984/12/31/201.

[2] C. Noguera, J. Goniakowski, Polarity in oxide ultrathin films, J. Phys.: Condens. Matter 20 (26) (2008) 264003, http://dx.doi.org/10.1088/0953-8984/20/26/264003.

[3] C.A. Cadigan, A.R. Corpuz, F. Lin, C.M. Caskey, K.B.H. Finch, X. Wang, R.M. Richards, Nanoscale (111) faceted rock-salt metal oxides in catalysis, Catal. Sci. Technol. 3 (4) (2013) 900, http://dx.doi.org/10.1039/c2cy20373a.

[4] V.K. Lazarov, R. Plass, H.-C. Poon, D.K. Saldin, M. Weinert, S.A. Chambers, M. Gajdardziska-Josifovska, Structure of the hydrogen-stabilized MgO(111)-(1x1) polar surface: Integrated experimental and theoretical studies, Phys. Rev. B 71 (11) (2005) 115434, http://dx.doi.org/10.1103/PhysRevB.71.115434.

[5] V.K. Lazarov, Z. Cai, K. Yoshida, K.H.L. Zhang, M. Weinert, K.S. Ziemer, P.J. Hasnip, Dynamically stabilized growth of polar oxides: The case of MgO(111), Phys. Rev. Lett. 107 (5) (2011) 056101, http://dx.doi.org/10.1103/PhysRevLett.107.056101.

[6] J. Mayer, C. Elsässer, M. Fähnle, Concentrations of atomic defects in B2-FexAl1-x. An ab-initio study, 191 (2) 283–298, http://dx.doi.org/10.1002/pssb.2221910205.

[7] B. Meyer, M. Fähnle, Atomic defects in the ordered compound *B*2-NiAl: A combination of ab initio electron theory and statistical mechanics, 59 (9) 6072–6082, http://dx.doi.org/10.1103/PhysRevB.59.6072.

[8] M. Rasamny, M. Weinert, G.W. Fernando, R.E. Watson, Electronic structure and thermodynamics of defects in $NiAl_3$, 64 (14) 144107, http://dx.doi.org/10.1103/PhysRevB.64.144107.

[9] A. Wander, I.J. Bush, N.M. Harrison, Stability of rocksalt polar surfaces: An ab initio study of MgO(111) and NiO(111), 68 (23) 233405, http://dx.doi.org/10.1103/PhysRevB.68.233405.

[10] F. Finocchi, A. Barbier, J. Jupille, C. Noguera, Stability of rocksalt (111) polar surfaces: Beyond the octopole, 92 (13) 136101, http://dx.doi.org/10.1103/PhysRevLett.92.136101.

[11] W.-B. Zhang, B.-Y. Tang, Stability of MgO(111) polar surface: Effect of the environment, 112 (9) 3327–3333, http://dx.doi.org/10.1021/jp077030+.

[12] E. Wimmer, H. Krakauer, M. Weinert, A.J. Freeman, Full-potential self-consistent linearized-augmented-plane-wave method for calculating the electronic structure of molecules and surfaces: $O_2$ molecule, 24 (2) 864–875, http://dx.doi.org/10.1103/PhysRevB.24.864.

[13] M. Weinert, E. Wimmer, A.J. Freeman, Total-energy all-electron density functional method for bulk solids and surfaces, 26 (8) 4571–4578, http://dx.doi.org/10.1103/PhysRevB.26.4571.

[14] M. Weinert, G. Schneider, R. Podloucky, J. Redinger, FLAPW: Applications and implementations, 21 (8) 084201, http://dx.doi.org/10.1088/0953-8984/21/8/084201.

[15] J.P. Perdew, K. Burke, M. Ernzerhof, Generalized gradient approximation made simple, Phys. Rev. Lett. 77 (18) (1996) 3865–3868, http://dx.doi.org/10.1103/PhysRevLett.77.3865.

[16] G. Kresse, J. Hafner, Ab initio molecular dynamics for liquid metals, 47 (1) 558–561, http://dx.doi.org/10.1103/PhysRevB.47.558.

[17] G. Kresse, J. Furthmüller, Efficiency of ab-initio total energy calculations for metals and semiconductors using a plane-wave basis set, Comput. Mater. Sci. 6 (1) (1996) 15–50, http://dx.doi.org/10.1016/0927-0256(96)00008-0.

[18] G. Kresse, J. Furthmüller, Efficient iterative schemes for ab initio total-energy calculations using a plane-wave basis set, Phys. Rev. B 54 (16) (1996) 11169–11186, http://dx.doi.org/10.1103/PhysRevB.54.11169.

[19] G. Kresse, D. Joubert, From ultrasoft pseudopotentials to the projector augmented-wave method, Phys. Rev. B 59 (3) (1999) 1758–1775, http://dx.doi.org/10.1103/PhysRevB.59.1758.

[20] A. Rohrbach, J. Hafner, G. Kresse, Molecular adsorption on the surface of strongly correlated transition-metal oxides: A case study for CO/NiO(100), Phys. Rev. B 69 (7) (2004) 075413, http://dx.doi.org/10.1103/PhysRevB.69.075413.

[21] E. Kaxiras, K.C. Pandey, Y. Bar-Yam, J.D. Joannopoulos, Role of chemical potentials in surface reconstruction: A new model and phase transition of GaAs(111)2x2, 56 (26) 2819–2822, http://dx.doi.org/10.1103/PhysRevLett.56.2819.

[22] G.-X. Qian, R.M. Martin, D.J. Chadi, First-principles study of the atomic reconstructions and energies of Ga- and As-stabilized GaAs(100) surfaces, 38 (11) 7649–7663, http://dx.doi.org/10.1103/PhysRevB.38.7649.

[23] X.-G. Wang, W. Weiss, S.K. Shaikhutdinov, M. Ritter, M. Petersen, F. Wagner, R. Schlögl, M. Scheffler, The hematite ($\alpha$-$Fe_2O_3$) (0001) surface: Evidence for domains of distinct chemistry, 81 (5) 1038–1041, http://dx.doi.org/10.1103/PhysRevLett.81.1038.

[24] A. Pojani, F. Finocchi, C. Noguera, Polarity on the SrTiO3 (111) and (110) surfaces, 442 (2) 179–198, http://dx.doi.org/10.1016/S0039-6028(99)00911-5.

[25] I.G. Batyrev, A. Alavi, M.W. Finnis, Equilibrium and adhesion of Nb/sapphire: The effect of oxygen partial pressure, 62 (7) 4698–4706, http://dx.doi.org/10.1103/PhysRevB.62.4698.

[26] K. Reuter, M. Scheffler, Composition, structure, and stability of $RuO_2$(110) as a function of oxygen pressure, 65 (3) 035406, http://dx.doi.org/10.1103/PhysRevB.65.035406.

[27] K. Reuter, M. Scheffler, First-principles atomistic thermodynamics for oxidation catalysis: Surface phase diagrams and Catalytically Interesting Regions, 90 (4) 046103, http://dx.doi.org/10.1103/PhysRevLett.90.046103.

[28] B. Meyer, First-principles study of the polar O-terminated ZnO surface in thermodynamic equilibrium with oxygen and hydrogen, 69 (4) 045416, http://dx.doi.org/10.1103/PhysRevB.69.045416.

[29] T.L. Goodrich, Z. Cai, K.S. Ziemer, Stability of MgO(111) films grown on 6H-SiC(0001) by molecular beam epitaxy for two-step integration of functional oxides, 254 (10) 3191–3199, http://dx.doi.org/10.1016/j.apsusc.2007.10.077.

[30] K. Matsuzaki, H. Takagi, H. Hosono, T. Susaki, Structural study of polar MgO(111) epitaxial thin films grown on $SrTiO_3$(111), 84 (23) 235448, http://dx.doi.org/10.1103/PhysRevB.84.235448.

[31] J. Ciston, A. Subramanian, L.D. Marks, Water-driven structural evolution of the polar MgO (111) surface: An integrated experimental and theoretical approach, Phys. Rev. B 79 (8) (2009) 085421.

[32] J. Ciston, A. Subramanian, D.M. Kienzle, L.D. Marks, Why the case for clean surfaces does not hold water: Structure and morphology of hydroxylated nickel oxide (111), Surf. Sci. 604 (2) (2010) 155–164, http://dx.doi.org/10.1016/j.susc.2009.10.033.

[33] S. Benedetti, N. Nilius, P. Torelli, G. Renaud, H.-J. Freund, S. Valeri, Competition between polar and nonpolar growth of MgO thin films on Au(111), 115 (46) 23043–23049, http://dx.doi.org/10.1021/jp207901a.